

Wave function recombination instability in cold atom interferometers

James A. Stickney and Alex A. Zozulya
Department of Physics, WPI, 100 Institute Road, Worcester, MA 01609

Cold atom interferometers use guiding potentials that split the wave function of the Bose-Einstein condensate and then recombine it. We present theoretical analysis of the wave function recombination instability that is due to the weak nonlinearity of the condensate. It is most pronounced when the accumulated phase difference between the arms of the interferometer is close to an odd multiple of π and consists in exponential amplification of the weak ground state mode by the strong first excited mode. The instability exists for both trapped-atom and beam interferometers.

PACS numbers: 03.75.-b, 39.20.+q, 03.75.Be

Recent experimental demonstrations of miniature cold atom guides [1, 2, 3, 4], beam splitters [5, 6, 7, 8], and Bose-Einstein condensation (BEC) on a chip [9] open the possibility of ultra-precise inertial and rotation measurements via cold atom interferometry. Cold atom interferometers split the wave function of the condensate and then recombine it by using guiding potentials that change from a single well into two separate wells and back. Both the splitting and recombination are adiabatically slow to avoid excitation of unwanted modes. The phase of the wave function in each of the two potential wells evolves independently once the wells are separated far enough and is sensitive to its local environment. As a consequence, these two wave functions acquire a relative accumulated phase difference ϕ . When the two potential wells converge back to a single well, this phase difference results in an interference that is used to extract information about the differences between local environments.

In this paper we present theoretical analysis of the wave function recombination instability that is due to the weak nonlinearity of the condensate. It is most pronounced when the relative phase difference ϕ is close to an odd multiple of π . The instability consists in exponential amplification of the weak ground state (symmetric) mode by the strong first excited (antisymmetric) mode. We calculate the instability growth rate and present its dependence on the shape of the guiding potential and the nonlinearity for both trapped-atom and beam interferometers.

Evolution of the condensate in the interferometer will be described by a one or two-dimensional nonlinear Schrodinger equation (NLSE)

$$i\frac{\partial}{\partial t} \psi(x; t) = -\frac{1}{2} \frac{\partial^2}{\partial x^2} \psi(x; t) + V(x; t) + N \left| \psi(x; t) \right|^2 \psi(x; t); \quad (1)$$

The wave function ψ in Eq. (1) is normalized to unity, V is the linear guiding potential, time is normalized to the characteristic eigenfrequency ω_0 of this potential, and the spatial coordinates are normalized to the characteristic length $a_0 = (\hbar \omega_0 M)^{1/2}$, where M is the atom mass. Finally, N is the normalized nonlinearity parameter.

In its one-dimensional form, $x = x$, Eq. (1) describes a trapped-atom interferometer [10, 11]. The condensate

is tightly confined in two transverse dimensions and is in the lowest transverse mode of the trap. Equation (1) is the projection of the Gross-Pitaevskii equation onto this lowest transverse mode. The nonlinearity parameter N contains the overlap integral between the three-dimensional wave function of the condensate and the lowest transverse eigenmode of the trap and is, in general, time-dependent. In our analysis we assume $N = \text{const}$. Generalizations to the time-dependent nonlinearity parameter N are straightforward.

In its two-dimensional form, $x = (x; y)$, Eq. (1) describes a beam interferometer [12, 13]. Here the condensate cloud propagates along the z -axis in the guiding potential $V(x; y; z)$ that confines the condensate in the x - y plane. Equation (1) is written in a co-propagating frame that is moving with the condensate. The time dependence of the guiding potential $V(x; y; t)$ is then parameterized by the longitudinal velocity of the condensate v : $V(x; y; t) = V(x; y; z_0 + vt)$. The conditions of applicability of Eq. (1) are

$$M v = h = k_p \quad M l_0 = h^{1/2} \quad (2)$$

and

$$k_p l_0 \ll 1; \quad (3)$$

where M is the atom mass and l_0 is the characteristic spatial scale of the guiding potential $V(x; y; z)$ along the z axis. The first inequality means that the energy associated with the longitudinal motion of the condensate is much larger than the characteristic energy $h l_0$ of transverse eigenmodes of the interferometer. The second inequality ensures that undesirable backward reflections of the condensate wave function from the guiding potential are exponentially small and can be neglected. Additionally, this inequality allows one to neglect the $\partial^2 \psi / \partial z^2$ term in Eq. (1).

We start our analysis from the one-dimensional version of Eq. (1) with the simple model guiding potential of the form

$$V(x; t) = 1 + (t - x^2/2)^2^{-1/2}; \quad (4)$$

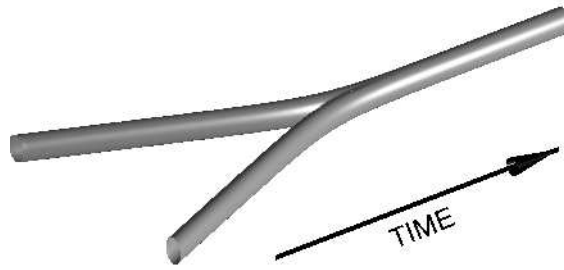


FIG. 1: Schematic view of the recombination region.

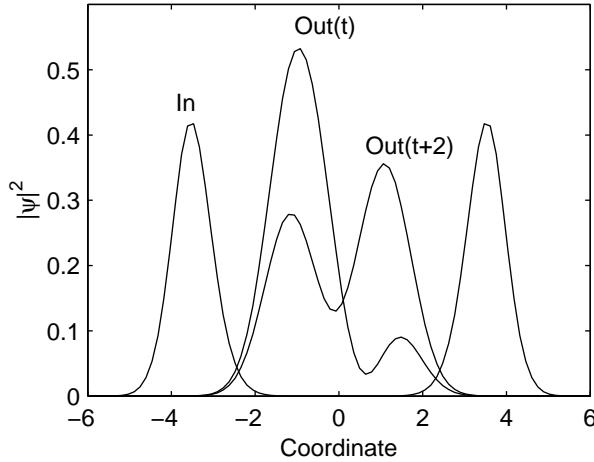


FIG. 2: Condensate density before and after the recombination.

where $\alpha(t)$ is the control parameter. A zero value of α corresponds to a single potential well of the potential V . Positive values of α split the potential V into two wells separated by the distance $d = 2(2\alpha)^{1/2}$.

We assume that the condensate is initially in the lowest weakly nonlinear mode of the single-well potential $V(\alpha = 0)$ with the value of the chemical potential that is about 12% higher than the eigenenergy of the lowest linear eigenmode $\lambda_1 = 1.3$. This value of α corresponds to the nonlinearity parameter $N = 0.5$ in Eq. (1). We further assume that the condensate wave function is split by increasing the control parameter α and acquires a relative phase shift $\phi = 2 \times 10^2$ before the recombination. The recombination stage is modelled by choosing the control parameter $\alpha(t)$ to be of the form

$$\alpha(t) = A \ln[\exp(-t/T) + 1]; \quad (5)$$

where A and T are constants. Equation (5) describes two separate wells that are linearly converging toward each other at large negative values of time and merging at large positive values of time. The schematic view of the recombination region is shown in Fig. 1. Figure 2 shows the condensate density before and after the recombination. The initial wave function is the combination of the lowest weakly nonlinear eigenmodes of the left and right

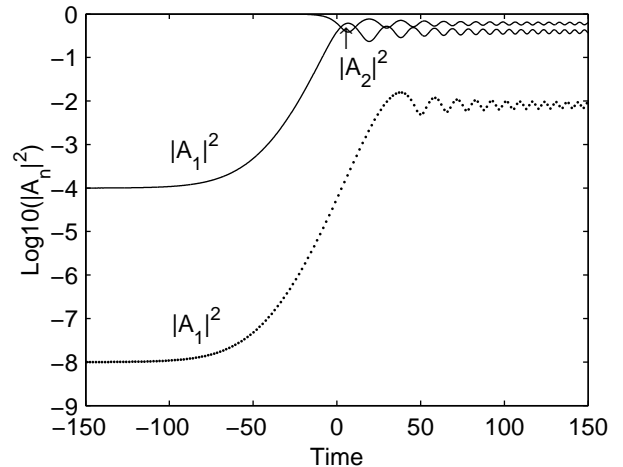


FIG. 3: Modal decomposition coefficients versus time. A_1 is the ground state mode and A_2 is the first excited mode of the guiding potential V .

potential wells with the relative phase shift ϕ , i.e., the first antisymmetric weakly nonlinear eigenmode of the potential V . Because the nonlinearity is weak, this mode practically coincides with the first antisymmetric linear mode of the potential V . The fractional contributions of the higher antisymmetric linear modes are about 10^{-4} . Additionally, the input wave function contains a small amount of the first linear symmetric mode of the potential V at the level of 10^{-4} . The parameters used for this calculation are $A = 3$ and $T = 90$.

The value of the parameter $T = 90$ ensures that the recombination is adiabatic and hence the input wave function should map onto the lowest antisymmetric mode of the single-well potential $V(\alpha = 0)$ preserving its odd parity. Figure 2 instead demonstrates that the parity is broken and the wave function after the recombination is a superposition of even and odd modes. To quantify this statement we introduce modal decomposition coefficients $A_n(t)$ of the wave function $\psi(x; t)$ onto linear eigenmodes $\lambda_n(x; \alpha)$ of the potential V by the relations

$$\begin{aligned} \psi(x; t) &= \sum_{n=0}^{\infty} A_n(t) \lambda_n(x; \alpha(t)); \\ A_n(t) &= \int dx \psi(x; t) \lambda_n(x; \alpha(t)); \end{aligned} \quad (6)$$

The linear eigenmodes of the potential $V(\alpha; \alpha)$ and their eigenfrequencies λ_n are solutions of the eigenvalue problem

$$\lambda_n(x; \alpha) = -\frac{1}{2} \frac{d^2}{dx^2} \psi(x; \alpha) + V(x; \alpha) \psi(x; \alpha) \quad (7)$$

and parametrically depend on the control parameter α . Figure 3 shows modal decomposition coefficients $|A_1|^2$ and $|A_2|^2$ as functions of time on a logarithmic scale.

Solid lines correspond to the results shown in Fig. 2. The input wave function shown in Fig. 2 corresponds to $\mathcal{A}_2 \hat{f} = 1$ and $\mathcal{A}_1 \hat{f} = 10^4$. Figure 3 clearly demonstrates exponential amplification of the weak mode 1 at the expense of the strong mode 2 until mode 2 is depleted. The dotted curve in Fig. 3 corresponds to a run with the same parameters except the initial population of the first mode was chosen to be $= 10^8$. This curve shows that the instability exists only in some range of the control parameter β . If this parameter is above or below certain values, the system is stable. Indeed, in the run with $= 10^8$ the first mode stabilizes at the value of 10^2 after 40 despite the fact that mode 2 (not shown) remains undepleted.

To get an insight into the nature of the instability, we fix the control parameter at some constant value and replace Eq. (1) by a set of coupled equations for the modal amplitudes $A_n(t)$

$$i \frac{d}{dt} A_n = \omega_n A_n + N \sum_{k \neq m} \text{Im} A_k A_1 A_m : \quad (8)$$

Here

$$Z = \sum_{n \neq k \neq m} \text{Im} A_n A_k A_m : \quad (9)$$

are the intermodal overlap integrals.

Keeping only A_1 and A_2 in Eq. (8) results in the set of two coupled equations

$$\begin{aligned} i \frac{d}{dt} A_1 &= \omega_1 A_1 + N \omega_{1111} \mathcal{A}_1 \hat{f} A_1 \\ &+ 2 \omega_{1222} \mathcal{A}_2 \hat{f} A_1 + \omega_{1122} A_2^2 A_1 ; \\ i \frac{d}{dt} A_2 &= \omega_2 A_2 + N \omega_{2222} \mathcal{A}_2 \hat{f} A_2 \\ &+ 2 \omega_{1122} \mathcal{A}_1 \hat{f} A_2 + \omega_{1122} A_1^2 A_2 : \end{aligned} \quad (10)$$

Introducing new variables $y_1 = 2R\text{e}A_1A_2$, $y_2 = 2\text{Im}A_1A_2$ and $y_3 = \mathcal{A}_1 \hat{f} - \mathcal{A}_2 \hat{f}$ transforms Eq. (10) to the form

$$\begin{aligned} \frac{d}{dt} y_1 &= [\omega_1 + N K_1 + N K_2 y_3] y_2 ; \\ \frac{d}{dt} y_2 &= [\omega_2 - N K_1 - N K_3 y_3] y_1 ; \\ \frac{d}{dt} y_3 &= -N K_4 y_1 y_2 ; \end{aligned} \quad (11)$$

where

$$\begin{aligned} \omega &= \omega_2 - \omega_1 ; \\ K_1 &= \frac{1}{2} (\omega_{1111} - \omega_{2222}) ; \\ K_2 &= \frac{1}{2} (\omega_{1111} + \omega_{2222} - 2 \omega_{1122}) ; \\ K_3 &= \frac{1}{2} (\omega_{1111} + \omega_{2222} - 6 \omega_{1122}) ; \\ K_4 &= 2 \omega_{1122} ; \end{aligned} \quad (12)$$

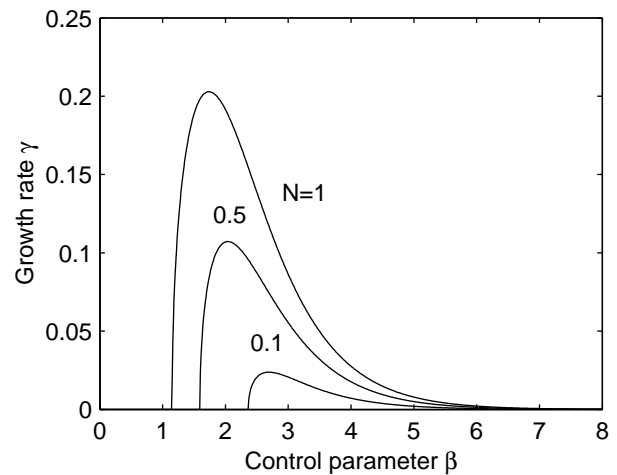


FIG. 4: Instability growth rate for a trapped-atom interferometer versus control parameter for several values of the nonlinearity N .

Equations (11) have two integrals of motion

$$\begin{aligned} y_1^2 + y_2^2 + y_3^2 &= 1 ; \\ N K_4 y_1^2 + 2 [\omega_1 + N K_1] y_3 + N K_2 y_3^2 &= c ; \end{aligned} \quad (13)$$

where c an integration constant, and can be solved in terms of elliptic functions. In the following we will be interested in the limit when the amplitude of A_2 (the first odd eigenmode) is much larger than that of A_1 (the first even eigenmode). This limit corresponds to $y_{1,2} \approx 0$, $y_3 \approx 1$ in Eq.(11) and yields solutions of the first two Eq. (11) of the form $y_1, y_2 \approx \exp(-t)$ with given by the relation

$$\begin{aligned} \omega &= [\omega_1 + N (\omega_{1122} - \omega_{2222})] \\ &[\omega_2 + N (\omega_{2222} - 3 \omega_{1122})] : \end{aligned} \quad (14)$$

The instability corresponds to $\omega^2 > 0$.

Both the eigenfrequencies ω and the overlap integrals in Eq. (14) depend on the shape of the guiding potential V , i.e., on the value of the control parameter β . Figure 4 shows the instability growth rate as a function of the control parameter β for different values of the nonlinearity N . The curves were obtained by solving the eigenvalue problem Eq. (7) and then calculating the growth rate according to Eq. (14).

For each curve plotted in Fig. 4 there exists a cut-off value of the control parameter below which the system is stable. These results explain saturation of the dotted curve in Fig. 3. The maximum growth rate corresponds to the values of β of the order of one. For large values of β the growth rate becomes exponentially small and scales as $\sim 1/\beta$. The asymptotic value corresponds to the frequency difference ω being exponentially small and to all the overlap integrals being exponentially close to each other. A nalytical estimates

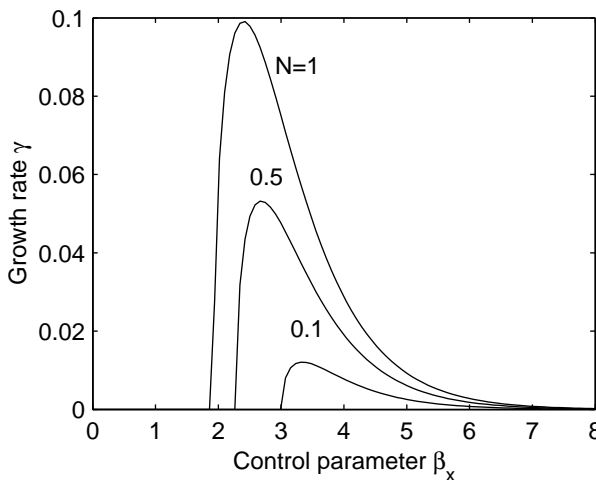


FIG. 5: Instability growth rate for a beam interferometer versus control parameter β_x for several values of the nonlinearity N .

carried out in the framework of a model of two identical square wells show that formally there exists no upper boundary on the separation between the wells that makes β_x^2 negative. From the practical point of view though the instability is quenched once the wells are sufficiently separated because the growth rate becomes exponentially small.

The preceding analysis has also been carried out with other shapes of the guiding potential V and gave similar results. Furthermore, the recombination instability also exists in the case of beam interferometers with two-dimensional guiding. Results of the previous modal analysis are straightforwardly carried over to this case. The instability growth rate is still given by the Eq. (14). The only difference is that one has to use the two-dimensional version of the eigenvalue problem Eq. (7).

Figure 5 shows the instability growth rate for the guiding potential

$$V(x; y) = [b_x^2(x; y) + b_y^2(x; y) + b_z^2]^{1/2}; \quad (15)$$

where

$$\begin{aligned} b_x &= x + \frac{1}{2}(y^2 - x^2); \\ b_y &= xy; \\ b_z &= 1; \end{aligned} \quad (16)$$

Equation (15) describes the guiding potential for the two-wire cold atom interferometer [13] in the limit when the characteristic size of the wave function is much smaller than the spatial scale of change of the magnetic field. The $x < 0$ part of the graph is the mirror reflection of the

$x > 0$ part and is not shown. Comparison of Fig. 4 and 5 shows that the instability exhibits similar qualitative behavior both in one- and two-dimensional cases.

Results of the preceding analysis demonstrate fascinating dynamics of weakly nonlinear guided matter waves and offer some insight into the design of cold atom interferometers. First, the guiding potential should not be made "too adiabatic". Changing the value of T from $T = 90$ to $T = 30$ ($T = 10$) in Eq. (5) reduces the total amplification of the weak mode from about 10^6 to 10^2 (10^1) while still preserving the adiabaticity. Secondly, the control parameter should be chosen in such a way as to minimize the time the wave function spends in the region with the largest instability growth rate. Finally, the instability analysis results can be used to estimate practical sensitivity of the interferometer in terms of errors of determining the phase difference for a given level of the nonlinearity.

This work was supported by the U.S. Army Research Office Multidisciplinary University Research Initiative.

zozulya@wpiedu

- [1] J. Denschlag, D. Cassetta, and J. Schmidmayer, Phys. Rev. Lett. 82, 2014 (1999).
- [2] D. M. Uller, D. Z. Anderson, R. J. Graw, P. D. D. Schwindt, and E. A. Cornell, Phys. Rev. Lett. 83, 5194 (1999).
- [3] N. H. Dekker, C. S. Lee, V. Lorent, J. H. Thywissen, S. P. Smith, M. D. Madic, R. M. Westervelt, and M. P. Prentiss, Phys. Rev. Lett. 84, 1124 (2000).
- [4] M. Key, I. G. Hughes, W. R. Roijakkers, B. E. Sauer, and E. A. Hinds, D. J. Richardson, and P. G. Kuznetsov, Phys. Rev. Lett. 84, 1371 (2000).
- [5] D. Cassetta, B. Hessmo, R. Folman, T. M. Mair, and J. Schmidmayer, Phys. Rev. Lett. 85, 5483 (2000).
- [6] D. M. Uller, E. A. Cornell, M. P. Prevedelli, P. D. D. Schwindt, A. Zozulya, and D. Z. Anderson, Opt. Lett. 25, 1382 (2000).
- [7] D. M. Uller, E. A. Cornell, M. P. Prevedelli, P. D. D. Schwindt, Y. J. Wang, and D. Z. Anderson, Phys. Rev. A 63, 041602(R) (2001).
- [8] O. Houdre, D. Kadio, and L. P. Puvost, Phys. Rev. Lett. 85, 5543 (2000).
- [9] W. Hansel, P. Hommelho, T. W. Hansch, and J. Reichel, Nature 413, 498 (2001).
- [10] W. Hansel, J. Reichel, P. Hommelho, and T. W. Hansch, Phys. Rev. A 64, 063607 (2001).
- [11] J. Reichel, W. Hansel, P. Hommelho, and T. W. Hansch, Appl. Phys. B 72, 81 (2001).
- [12] E. A. Andersson, T. Calarco, R. Folman, M. A. Andersson, B. Hessmo, and J. Schmidmayer, Phys. Rev. Lett. 88, 100401 (2002).
- [13] E. A. Hinds, C. J. Vale, and M. G. Boshier, Phys. Rev. Lett. 86, 1462 (2001).